NOTES AND CORRESPONDENCE

Global Ocean Meridional Overturning

RICK LUMPKIN

Physical Oceanography Division, NOAA/Atlantic Oceanographic and Meteorological Laboratory, Miami, Florida

KEVIN SPEER

Department of Oceanography, The Florida State University, Tallahassee, Florida

ABSTRACT

A decade-mean global ocean circulation is estimated using inverse techniques, incorporating air–sea fluxes of heat and freshwater, recent hydrographic sections, and direct current measurements. This information is used to determine mass, heat, freshwater, and other chemical transports, and to constrain boundary currents and dense overflows. The 18 boxes defined by these sections are divided into 45 isopycnal (neutral density) layers. Diapycnal transfers within the boxes are allowed, representing advective fluxes and mixing processes. Air–sea fluxes at the surface produce transfers between outcropping layers. The model obtains a global overturning circulation consistent with the various observations, revealing two global-scale meridional circulation cells: an upper cell, with sinking in the Arctic and subarctic regions and upwelling in the Southern Ocean, and a lower cell, with sinking around the Antarctic continent and abyssal upwelling mainly below the crests of the major bathymetric ridges.

1. Introduction

Wind, and heat and freshwater fluxes at the ocean surface are, together with tidal and other energy sources, responsible for the global ocean circulation, mixing, and the formation of a broad range of water masses. To attempt to distinguish key processes acting in the ocean these forcing terms may be analyzed dynamically or thermodynamically for constraints, such as Ekman transport and surface transformation, on ocean circulation. Such constraints are only useful if the errors are known and limited, in which case they may help to determine ocean transports. A number of air–sea exchange estimates, or datasets, have been derived variously from satellite and/or in situ observations and operational forecasting models, and are employed by researchers to investigate circulation and mixing

(WGASF 2001; Garnier et al. 2000; Josey 2001; Josey et al. 1999). The global pattern of wind and heat gain and loss in these products is qualitatively consistent in the Northern Hemisphere where the ocean gains heat in the Tropics and loses large amounts of heat in the northern North Atlantic. This heat loss is associated with the formation of mode waters, culminating in Labrador Sea Water, as well as the formation of dense overflows leading to North Atlantic Deep Water (NADW) and the development of the Atlantic overturning circulation.

In the subpolar Southern Ocean, discrepancies between flux datasets are larger. The ocean appears to gain heat over a large zone near 45°–50°S, although errors are large and the net flux is not well determined [WGASF (2001); all products used in this study contain heat gain here except the adjusted National Oceanography Centre product described by Grist and Josey (2003)]. It has been suggested that a region of high-latitude heat gain in both hemispheres is the natural result of the drop in latent heat fluxes as SST decreases rapidly across subpolar fronts (Wacongne et al. 2003). In the Southern Ocean, buoyancy fluxes associated

Corresponding author address: Dr. Rick Lumpkin, Physical Oceanography Division, NOAA/Atlantic Oceanographic and Meteorological Laboratory, 4301 Rickenbacker Causeway, Miami, FL 33149.
E-mail: rick.lumpkin@noaa.gov

with freshwater input (e.g., Warren et al. 1996) and heat gain convert upwelling water into less dense Subantarctic Mode Water (SAMW) classes in an upper diabatic overturning cell (Speer et al. 2000).

At the highest densities and latitudes, intense heat loss in the Norwegian Sea, Weddell Sea, and Ross Sea and in coastal polynyas generates dense overflows, some of which lead to large-scale water masses such as Lower North Atlantic Deep Water (LNADW) and Antarctic Bottom Water (AABW). This heat loss is poorly resolved in most flux products, but in the inverse model described here new Weddell Sea and Ross Sea outflow constraints, along with various constraints from observations of Greenland–Scotland overflow (Lumpkin and Speer 2003; hereafter LS03), produce surface transformation from air–sea fluxes consistent with the primary dense overflow transports. The Mediterranean Outflow is not at high latitudes but is another example of very dense water input, and its contribution is part of the global model described here.

Our goal is to combine surface air–sea fluxes with interior ocean transport constraints to derive a consistent global ocean isopycnal and diapycnal circulation with error estimates, which can be used for studying watermass conversion or thermodynamics, the transport of dissolved gases and nutrients or other chemical species, and to study the consistency of inferred diapycnal fluxes with physically based parameterizations. A pole-to-pole model is needed to include the dominant sources of dense water as part of the solution. These extreme dense water sources, together with sources from intermediate-density ocean convection, are basic elements of the global overturning circulation. Here we present an estimate of the mean global overturning streamfunction and diapycnal transports over the approximately decadal period of observations. Its strengths are a strong connection to data and data-based inferences of ocean circulation, and high vertical resolution; its weaknesses include nonsynoptic observations, the limited exploration of possible states via the least squares technique, bias introduced by the data-based constraints and reference levels, and coarse horizontal resolution.

2. Methods

Hydrographic sections from the World Ocean Circulation Experiment (WOCE) observation period (Table 1) are used to divide the ocean into 18 boxes (Fig. 1). This geometry includes an Arctic Ocean box, three Southern Ocean boxes between 32° and 62°S, and four Antarctic boxes south of 62°S. Our choice of sections to use is motivated by the desire to include explicit in situ transport measurements at various choke points and to

TABLE 1. WOCE hydrographic sections. A composite section was constructed for Greenland–Scotland (LS03). A composite section along nominal latitude 62°S was constructed from WOCE S4 sections. Choke-point sections in Bering Strait and the Canadian Archipelago were constructed from hydrographic climatology (Gouretski and Jancke 1998).

	Name	Nominal location	When occupied
Atlantic	Ar18	Denmark Strait	Sep 1995
	Ar7	56°N	Sep 1992
	Ar19	48°N	Jul 1993
	Ar16	Gulf of Cadiz	Sep 1992
	A5	24°N	Jul–Aug 1992
	A8	11°S	Apr–May 1994
	A11	32°S	Dec 1992–Jan 1993
Indian	Ir6	Indonesia–Australia	Feb–Mar 1992
	I5	32°S	Nov–Dec 1987
Pacific	P1	48°N	Aug–Sep 1985
	P3	24°N	May–Jun 1985
	P6	32°S	May–Jul 1992
Southern	A21	Drake Passage	Jan–Feb 1990
	I6	30°E	Feb–May 1996
	Sr3	143°E	Jan 1994
	Sr4	Weddell Sea	Sep–Oct 1989
	S4	31.0°–55.2°W	Mar–Apr 1999
		3.1°–25.6°W	Feb 1990
		0°–118.5°E	Mar–Jun 1996
		121.4°–162.1°E	Jan 1995
		162.7°E–70.1°W	Feb–Mar 1992

attempt to resolve meridional overturning in the Southern Ocean. In each box, buoyancy-driven transformation at monthly mean isopycnal outcrops by air–sea fluxes is included explicitly. Outcropping density is determined from monthly mean sea surface temperature (corresponding to the air–sea flux product) and monthly mean salinity from Levitus and Boyer (1994).

Five different products are used to determine the range of plausible heat, freshwater, and momentum (Ekman) fluxes: da Silva et al. (1994); Josey et al. (1998); Grist and Josey (2003); the National Centers for Environmental Prediction–National Center for Atmospheric Research (NCEP–NCAR) reanalysis, version 2; and the 15-yr European Centre for Medium-Range Weather Forecasts reanalysis (ERA-15). Buoyancy transformation from these products is calculated as described in LS03, with the mean transformation from the five used to determine the preinverse diapycnal advection from one model layer to the next. Within each box, an inverse technique, Gauss–Markov estimation (Wunsch 1996, 179–202), is used to determine property-dependent diapycnal transfers, adjustments to thermal wind reference velocities, and air–sea fluxes that conserve mass, heat, salt anomalies with respect to 35 psu, and, in boxes north of 32°S, top-to-bottom integrated silicate in 45 neutral density (γ^n: Jackett and McDougall 1997) layers. Within each layer, mass is conserved
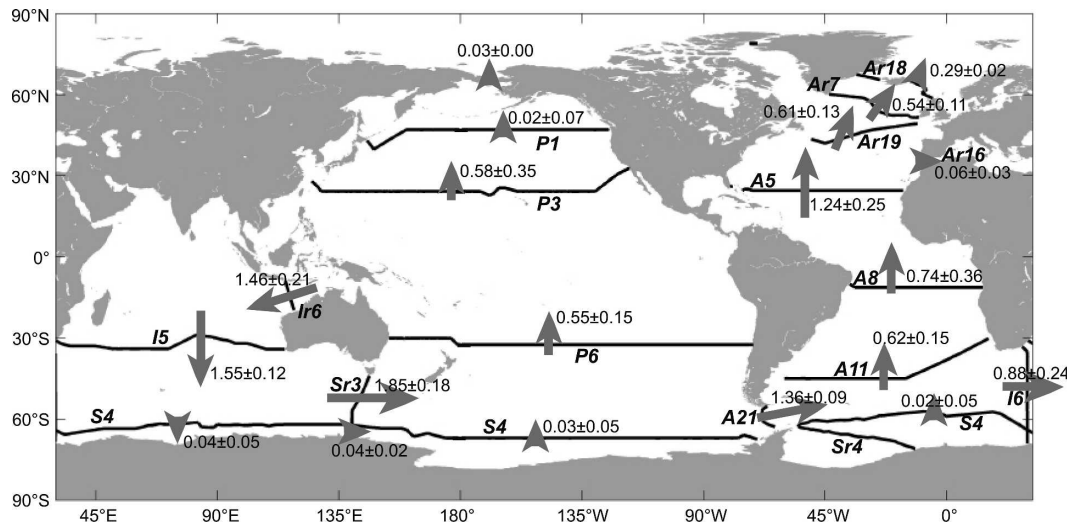
FIG. 1. Global box model geometry: 25 WOCE hydrographic sections (Table 1) form 18 boxes in which various properties are conserved and other constraints, such as the strengths of western boundary currents, are satisfied. Heat transports across the sections (red bars; units are 10^{15} W) are from the inverse model solution. Sections at a nominal latitude of 32°S separate the Atlantic, Indian, and Pacific basins from the Southern Ocean; a nearly circumpolar composite section at 62°S separates the bottom-water formation regions against Antarctica from the rest of the Southern Ocean.

to within ±1 Sv (Sv ≡ 10^6 m^3 s^{-1}) [see Ganachaud (2003a) for a detailed discussion of the sources of this model error]. Heat and salt anomaly conservation in the layers is constrained to within ±1 Sv times the sum of the mean property, plus twice the standard deviation of the property in the box (see appendix B in LS03). Net silicate is conserved to ±500 kmol s^{-1} in boxes north of 32°S. Each of the 45 model layers contains an equal volume of the world's water (LS03); 45 layers proved necessary to resolve the global range of water masses experiencing significant transformation. Previous observation-based studies of hydrographic sections have not included explicit air–sea buoyancy transformation (Ganachaud and Wunsch 2000; Talley et al. 2003; Ganachaud 2003b) or were not global (Sloyan and Rintoul 2001; LS03). The inversion presented here is also novel as it includes a circumpolar Southern Ocean section (WOCE S4) that helps distinguish transformation sites of the upper and lower meridional overturning cells.

Within the Arctic–Nordic seas box and Antarctic coastal margin boxes, none of the air–sea flux products includes sufficient ocean heat loss to accommodate the observed Denmark Strait and Faroe Banks overflows or Antarctic Bottom Water export across 62°S. In the ocean these fluxes are typically associated with relatively intense air–sea exchange in narrow boundary current regions or at small scales in leads and polynyas. Air–sea fluxes in these regions are not imposed upon the inverse solution and, instead, are derived via con-

straints on deep layer transports in various overflows and subbasins based on direct current measurements and tracer observations (Fahrbach et al. 1995; Orsi et al. 2002; LS03). In the case of the Weddell Sea we have reanalyzed direct current measurements (updated from Yaremchuk et al. 1998) to produce new boundary current constraints on circulation.

Interior diapycnal fluxes, reference velocity adjustments, and adjustments to the air–sea heat and freshwater fluxes are found that satisfy the imposed constraints. The model's adjusted air–sea heat fluxes are generally consistent within error to the products, with the following exceptions: unadjusted National Oceanography Centre (NOC) fluxes are too hot (ocean heat gain significantly larger than model results) in all tropical and subtropical boxes (cf., Grist and Josey 2003); adjusted NOC fluxes are too cold in all three Southern Ocean boxes (32°S–S4); NCEP fluxes are slightly too hot in Atlantic and Indian sectors of the Southern Ocean boxes; ERA-15 fluxes are too hot in the coastal Antarctica boxes and Arctic Sea box; and the University of Wisconsin—Milwaukee/Comprehensive Ocean–Atmosphere Data Set (UWM/COADS) fluxes are too cold in the Arctic box. Model-derived transports across key sections are given in Table 2. Net global meridional salt and volume (freshwater) fluxes are not well determined at any latitude. Net global ocean heat transports are consistent with earlier results within errors, which are typically of the same order as earlier studies. Unlike in the North Atlantic (LS03), where various air–sea flux

TABLE 2. Maximum overturning and net transports across hydrographic section locations (see Table 1). Values include geostrophic and Ekman transport. "G–I–S" values are for composite sections across the Greenland–Iceland–Scotland ridges including Ar18; "CanArch" is the Canadian Archipelago throughflow; "I–A" is the Indonesia–Australia section Ir6. Positive values are northward (eastward for I–A and Drake).

		Overturning (10^6 m^3 s^{-1})	Volume (10^6 m^3 s^{-1})	Salt (10^9 g s^{-1})	Heat (10^{15} W)
Atlantic	G–I–S	4.0 ± 0.7	-0.1 ± 0.3	2 ± 16	0.29 ± 0.02
	CanArch	—	-0.9 ± 0.2	-31 ± 7	0.00 ± 0.00
	56°N	17.0 ± 4.3	0.0 ± 0.8	7 ± 29	0.54 ± 0.11
	48°N	16.3 ± 2.7	-0.8 ± 1.2	-23 ± 46	0.61 ± 0.13
	24°N	18.0 ± 2.5	-0.4 ± 2.2	-5 ± 80	1.24 ± 0.25
	11°S	16.2 ± 3.0	-0.5 ± 2.5	-11 ± 95	0.74 ± 0.36
	32°S	12.4 ± 2.6	-0.2 ± 1.4	-3 ± 53	0.62 ± 0.15
Indian	I–A	—	-13.3 ± 1.8	-473 ± 65	-1.46 ± 0.21
	32°S	12.4 ± 2.6	-13.7 ± 2.6	-498 ± 95	-1.55 ± 0.12
Pacific	Bering	—	0.8 ± 0.1	29 ± 4	0.03 ± 0.00
	48°N	2.2 ± 1.5	0.4 ± 1.4	18 ± 50	0.02 ± 0.07
	24°N	5.1 ± 3.1	0.2 ± 2.6	12 ± 98	0.58 ± 0.35
	32°S	14.9 ± 3.4	14.3 ± 3.4	507 ± 124	0.55 ± 0.15
Southern	Drake	—	129.7 ± 6.8	4611 ± 246	1.36 ± 0.09
	30°E	—	131.7 ± 8.24	4676 ± 297	0.88 ± 0.24
	143°E	—	141.5 ± 11.4	5030 ± 414	1.85 ± 0.18
	Weddell	3.6 ± 2.3	1.5 ± 4.1	2 ± 53	0.02 ± 0.05
Circumpolar	48°N	17.2 ± 3.3	-0.4 ± 1.8	-5 ± 68	0.62 ± 0.08
	24°N	19.4 ± 3.7	-0.1 ± 3.6	7 ± 143	1.75 ± 0.19
	32°S	20.9 ± 6.7	0.4 ± 3.4	6 ± 162	-0.41 ± 0.18
	62°S	12.5 ± 4.0	0.6 ± 4.4	33 ± 485	0.02 ± 0.07

products have quantitatively similar values, the larger range of values in the Southern Ocean produces larger error bars on our global estimates. In the Pacific Ocean the heat transport is large and northward because of a relatively strong Pacific–Indonesian Throughflow (PIT). Unlike many earlier studies (cf., Robbins and Toole 1997), we find no significant heat divergence in the Indian Ocean north of 32°S, similar to Ganachaud and Wunsch (2000) and a consequence of the relatively strong (13.2 ± 1.8 Sv) PIT in our solution.

The global overturning circulation

Two global-scale counterrotating meridional cells dominate the inverse model solution's global overturning circulation (Fig. 2). Two smaller, shallow cells, present only in the isopycnal-averaged coordinates, are associated with subtropical gyres. These smaller cells are not adequately resolved in the present configuration of the model. The magnitude of the two principal cells is about the same, 17.2 ± 3.3 Sv (at 48°N) for the upper cell and 20.9 ± 6.7 Sv (at 32°S) for the lower cell. Dense overflows and outflows account for most of the lower cell and about half the upper cell.

On an imaginary meridional overturning trajectory following zonally averaged streamlines, buoyancy loss takes place at high Northern Hemisphere latitudes mainly in the surface layer but, in addition, some transformation takes place subsurface, such as in entrain-

ment associated with Greenland–Scotland overflows (LS03). As the deep water returns southward across subtropical and tropical latitudes, its density decreases due to mixing (streamlines rise across density levels in Fig. 2, top), eventually crossing 32°S at 27.0–27.6[1] γ^n and entering the circumpolar Southern Ocean. Within the Southern Ocean this water rises and is exposed to surface heating and northward Ekman transport, and flows northward to close the cell.

Water crossing 32°S southward at density greater than 27.6 γ^n outcrops near the Antarctic continent, flows southward, and is transformed into dense bottom water in the marginal seas of Antarctica before returning to the Southern Ocean. In our model, the amount of bottom water formed in the Weddell Sea (7.6 ± 4.4 Sv at $\gamma^n > 28.11$) is constrained by direct measurements, while the export of bottom water elsewhere is less tightly constrained (see the appendix). From 62°S to 32°S, very dense lower-cell streamlines converge in the density range 28.1–28.2 γ^n (Fig. 2, top), indicating mixing in the deep Antarctic Circumpolar Current (ACC). The downward transfer of ~9 Sv across 28.14 γ^n (the interface between lower deep water and ACC bottom water: Orsi et al. 2002) may be associated with entrain-

---

[1] Note that surface density values used in the air–sea flux transformation calculations are biased low because of the use of monthly climatologies for outcropping density within the boxes.
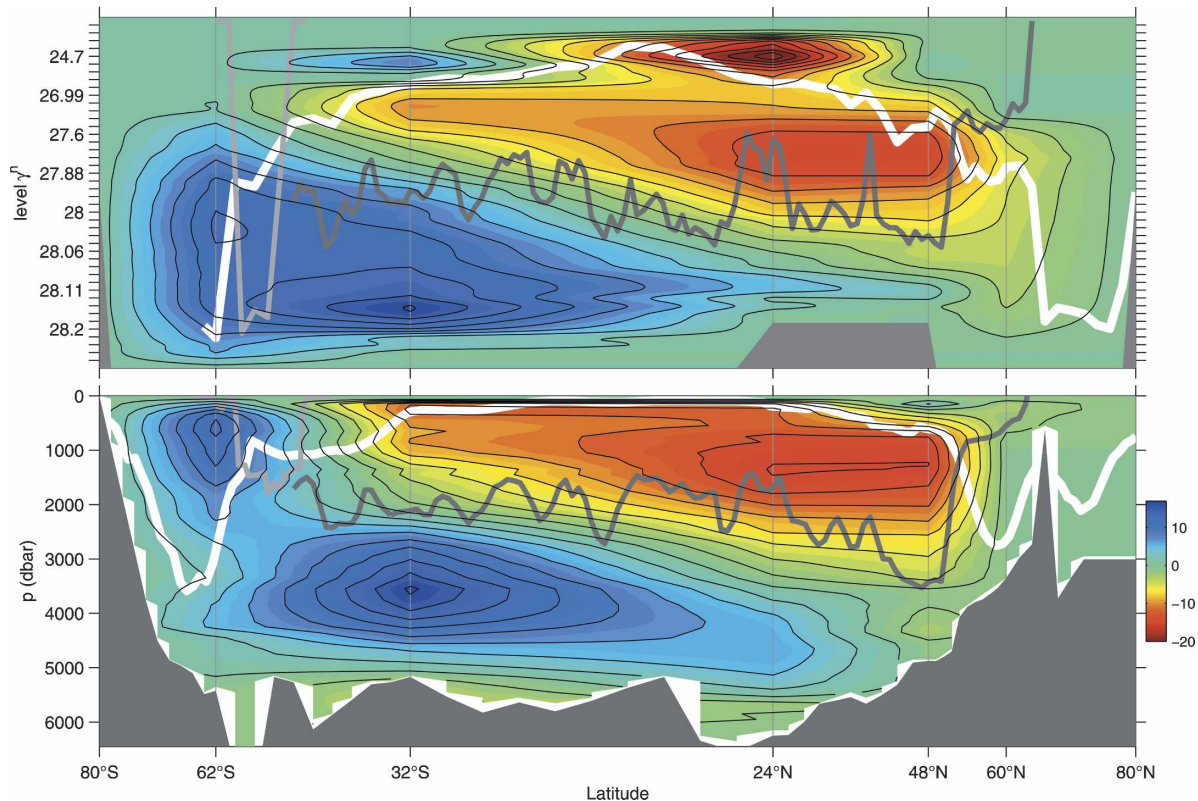
FIG. 2. Zonally averaged global overturning streamfunction (Sv; every 2 Sv contoured) in (top) density and (bottom) pressure levels across hydrographic sections (vertical gray lines) with linear interpolation between the sections. Typical winter mixed layer densities/depths (white), the mean depth of ocean ridge crests (dark gray), and the depth of the Scotia Arc east of Drake Passage (light gray) are also shown.

ment and topography-driven mixing in regions such as the Drake Passage/Scotia Sea (Garabato et al. 2003) or other locations on the Antarctic Mid-Ocean Ridge. This downwelling is, however, sensitive to the dense transport across 62°S; in an experimental inversion with a doubling of the northward export to 20 ± 1 Sv at $\gamma^n > 28.15$, imposed by constraint (control run produces 10 Sv), the downward transfer disappears and bottom-water transport across 32°S is fed entirely by transport across 62°S.

Dense water continues northward across 32°S into the Atlantic, Indian, and Pacific basins where it is transformed back to lighter water by abyssal diapycnal mixing. The net overturning across 32°S, at 20.9 ± 6.7 Sv, is close to previous estimates at this latitude (21 ± 6 Sv: Ganachaud 2003b; 22 Sv: Talley et al. 2003). This result is considerably smaller than the $O(50 \text{ Sv})$ overturning of Sloyan and Rintoul (2001), with the largest discrepancy in Upper Circumpolar Deep Water (UCDW: 27.4–28.0 γ^n) where we find 20 Sv globally southward across 32°S, as opposed to 52 Sv. While both our inverse model and that of Sloyan and Rintoul include explicit air–sea forcing, the two have been formulated

differently, particularly in how they treat the interaction of Ekman transport and watermass transformation. As noted in LS03, Sloyan and Rintoul's formulation can bias the formation rate high, and these model differences, rather than differences in air–sea fluxes, account for the disparate results. When forced by each of the five flux products in separate inversions, we find southward UCDW transport across 32°S ranges from a minimum of 15 Sv (adjusted NOC COADS; Grist and Josey 2003) to a maximum of 20 Sv (NCEP–NCAR reanalysis, version 2). In both this model and in Sloyan and Rintoul (2001), independent layer-to-layer transfers are allowed for each property: that is, we do not assume that a single effective diffusivity value acts to transfer both heat and salt between two neutral density layers in a given box. Thus, both studies have similar degrees of freedom in the regions where they overlap.

When the Atlantic and Indo–Pacific portions of the global overturning are examined separately (Fig. 3), a richer picture of the overturning circulation's structure emerges. The upper cell is predominantly associated with Atlantic overturning and buoyancy gain in the Southern Ocean, but—unlike in the globally averaged
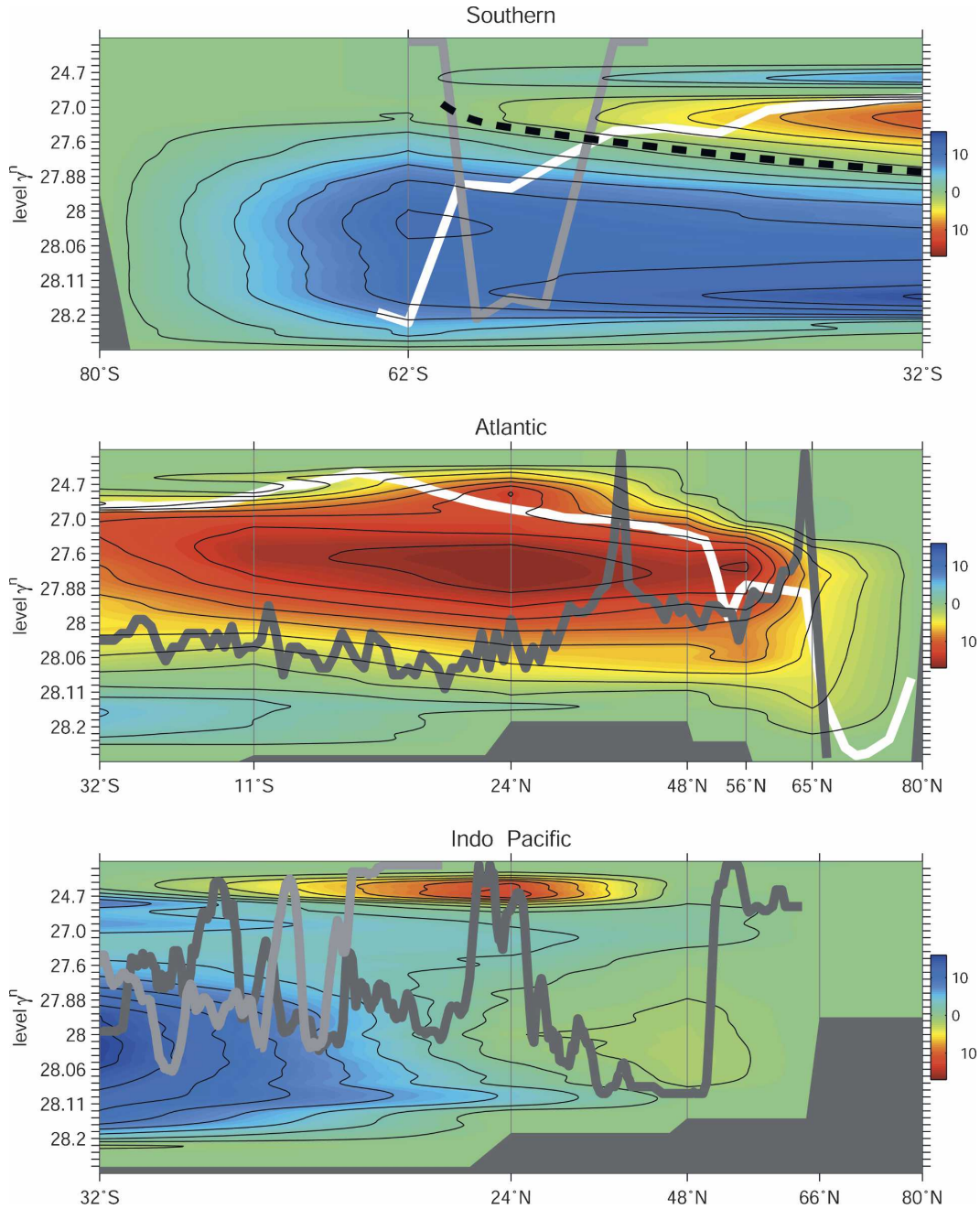
FIG. 3. Overturning circulation of the (top) Southern, (middle) Atlantic, and (bottom) Indo–Pacific Oceans in model-layer (density) coordinates. Dashed line in the Southern Ocean divides the upper and lower global overturning cells. Note that this dividing line outcrops (crosses the white line) roughly in the latitude range of Drake Passage. Gray lines indicate the crest of the Mid-Atlantic Ridge and major bathymetric features of the Pacific (dark) and Indian (light) Ocean basins and the Scotia Ridge of the Southern Ocean.

picture—is not a simple closed loop. Surface, thermocline, and intermediate-density water enters the North Atlantic and is ultimately transformed into North Atlantic Deep Water before reentering the Southern Ocean. Above the crest of the Mid-Atlantic Ridge (gray line in Fig. 3, middle) this water experi-

ences no significant diapycnal transformation. Beneath the NADW, 5.6 ± 3.0 Sv of Antarctic Bottom Water enters the Atlantic at 32°S and is ultimately transformed to NADW by diapycnal mixing at tropical and subtropical latitudes. The southward NADW export across 32°S is 17.9 ± 3.1 Sv in the density range 27.29–
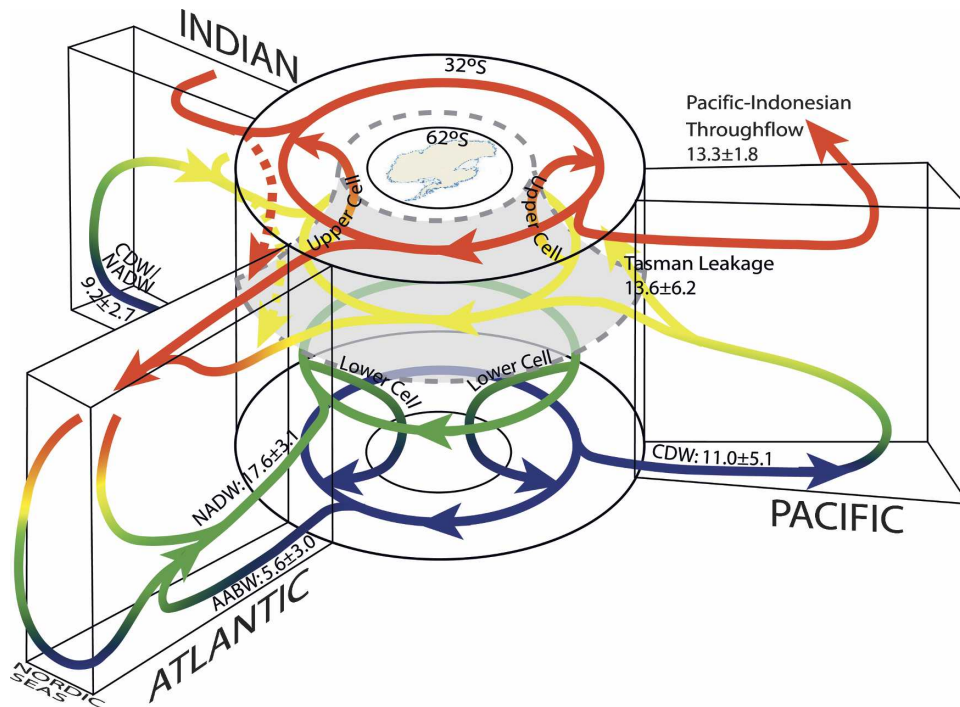
FIG. 4. Schematic of global overturning circulation. Color indicates approximate density ranges. Red: upper, $\gamma^n < 27.0$; yellow: intermediate, $\gamma^n \approx 27.0–27.6$; green: deep, $\gamma^n \approx 27.6–28.15$; blue: bottom, $\gamma^n > 28.15$. Gray surface with dashed edges is $\gamma^n = 27.6$ at 32°S, separating upper and lower cell transformation in the Southern Ocean (dashed line in Fig. 3, top). Dashed arrows indicate Indian-to-Atlantic westward exchange between Africa and the ACC. Shallow subtropical cells not included. Format adapted from Schmitz (1996).

28.18 γ^n, similar to previous estimates (e.g., Ganachaud 2003b; Talley et al. 2003).

Most (11 Sv, or about 75%) of the southward flow of NADW is at densities $\gamma^n > 27.6$ (black dashed line in Fig. 3; gray surface in Fig. 4). This value marks the average division between the upper and lower cells within the Southern Ocean, and roughly separates two distinct circulation regimes of the global ocean. Thus, the majority of the NADW cannot be exposed to the buoyancy-gaining transformation of the upper cell, but instead enters the lower cell and is transformed to yet denser bottom-water classes. Some becomes Atlantic AABW; the rest enters the Indian (12.4 ± 2.6 Sv) and Pacific (10.3 ± 5.1 Sv) basins as Circumpolar Deep Water (CDW: Fig. 4) and/or modified NADW. Abyssal mixing transforms this deep water to lighter density, $\gamma^n < 27.9$, before it returns southward across 32°S. At these densities, the water reenters the upper cell and is returned to the Atlantic via various routes (cf., Speich et al. 2002).

Southern Ocean air–sea fluxes roughly balance Ekman heat transport and transform outcropping water at $\gamma^n < 27.6$ into lighter mode water classes (Fig. 3; Speer et al. 2000). In experimental inversions with both air–

sea heat and freshwater fluxes set to zero south of 32°S, the model failed to find solutions sufficiently consistent with the imposed constraints—in other words, buoyancy gain is essential in the model to close the upper overturning cell. Southern Ocean mode waters are advected equatorward within the subtropical gyres and, in the Pacific and Atlantic, move into the Northern Hemisphere in western boundary currents, thus closing the global upper-cell recirculation.

3. Discussion

Our model connects all major World Ocean basins and explicitly accounts for all watermass formation. Despite the inclusion of explicit air–sea fluxes in our inverse model, and particular attention to direct estimates of transport where they exist, the error bars of the principal components of ocean transport—especially in Southern Ocean transports—are comparable to earlier studies. This is mainly due to uncertainties in air–sea fluxes, and improvements in these flux estimates could greatly improve the accuracy of our results.

Recent debate has focused upon the relative role of air–sea forcing versus subsurface mixing in the global
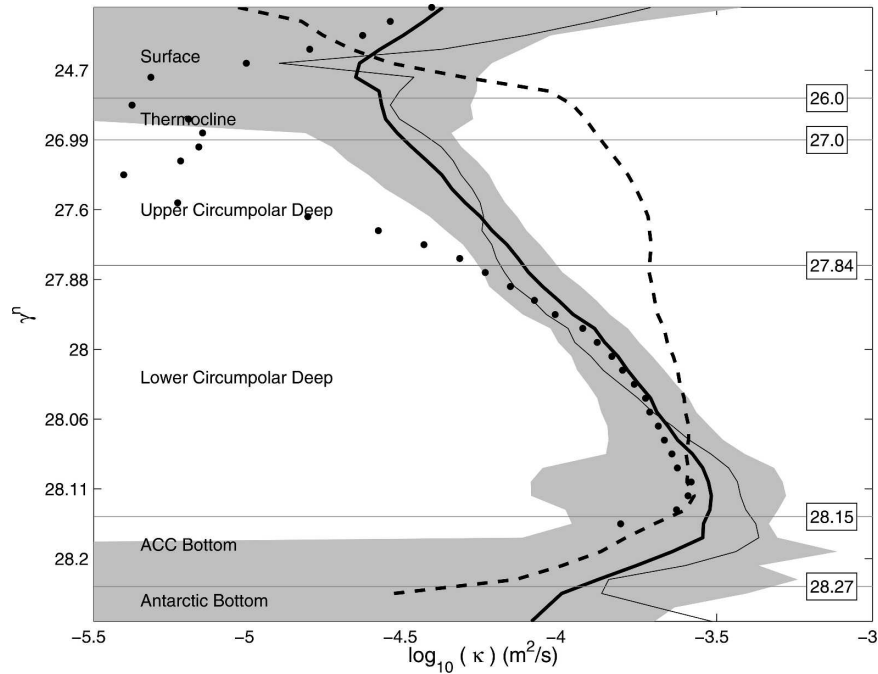
FIG. 5. Volume-averaged effective diapycnal diffusivity as a function of neutral density for all boxes between 32°S and 48°N (thick line with standard error shaded). Also shown are the profiles for the Atlantic (thin solid), Indian (dashed), and Pacific (dotted) boxes, 32°S–48°N. Horizontal lines indicate watermass divisions (Orsi et al. 2002).

overturning circulation (cf. Gnanadesikan 1999). In the model presented here, a large-scale averaged effective diapycnal diffusivity κ_{eff} may be estimated from interior layer transfers across neutral density surfaces, that is, not including diapycnal transformation driven by air–sea fluxes. Effective diffusivity values can be formulated from the area-averaged density flux across neutral density surfaces, as determined by the inversion, and from estimates of the mean area of these surfaces (estimated from hydrographic climatology: Gouretski and Jancke 1998). This formulation (cf. Speer 1997; Zhang and Talley 1998) of an effective diffusivity is not the same as the area-averaged mixing coefficient since it neglects possible covariations of layer thickness and diffusivity but expresses mixing intensity in familiar units. At high latitudes near dense marginal sea outflows and where layers outcrop, advective processes associated with eddies and mixing processes, such as entrainment, are widespread and confound a separation into a simple diffusion term and coefficient of mixing. At lower latitudes the global mean vertical structure of effective diffusivity determined from the inversion (Fig. 5) shows weak mixing from the base of the thermocline (26.0 γ^n, $\kappa_{\text{eff}} = 10^{-5}$ m^2 s^{-1}) down to about 27.6 γ^n. Average diffusion rises to a maximum of (3.0 $\pm$ 1.4) $\times$ 10^{-4} m^2 s^{-1} at 28.11 γ^n. This value is somewhat smaller than

previous inverse-derived estimates of diffusivity (cf., Ganachaud 2003b). Beneath thermocline densities these results are 3–15 times larger than globally averaged estimates based on lowered ADCP (LADCP) and CTD strain observations (Kunze et al. 2006).

Within error, our effective diffusivities are not distinguishable from Kunze et al.'s (2006) except in the density range 27.9–28.1 γ^n, where we find $\kappa_{\text{eff}} \approx 10^{-4}$ m^2 s^{-1} and they find somewhat smaller values of 1–3 ($\times$ 10^{-5} m^2 s^{-1}). Our larger values may reflect additional mixing on continental shelves, over topographic ridges, or in other regions not adequately sampled in the LADCP and CTD profiles of Kunze et al. (2006) and within hydraulic overflows (Price and Baringer 1994; Bryden and Nurser 2003) not sampled or accounted for in their methodology.

Buoyancy gain in the Southern Hemisphere can help account for the discrepancy between theoretical (Munk and Wunsch 1998) and observed (Toole et al. 1994; Kunze et al. 2006) mixing. We find that, on the global scale, air–sea forcing accomplishes much of the transformation within the upper-cell circulation so that buoyancy loss at high Northern Hemisphere latitudes is approximately balanced by buoyancy gain in the Southern Ocean. For this cell, outside of polar regions, interior diapycnal mixing is negligible near base-of-thermo-

cline densities to lowest order. On the other hand, mixing is significant in the upper cell, particularly in regions such as the shallow parts of dense overflows (LS03) and in outcropping layers where lateral eddy fluxes act in concert with air–sea forcing (Khatiwala et al. 2002). Such processes are not well distinguished from interior diffusion in the large boxes of the model, for instance in places where topography influences outcropping layers. They may be distinguishable in terms of their heat, salt, or other property fluxes, but quantitative statements probably require introducing an eddy flux parameterization to the model. Preliminary work has been started with eddy mass fluxes.

In contrast, the lower cell is fundamentally a balance between buoyancy gain by abyssal mixing (Fig. 5) and buoyancy loss by air–sea fluxes and boundary mixing. Again, the model does not resolve the processes responsible for the mixing, but rather represents the net mixing required by the circulation. The abyssal mixing mainly takes place within the range of direct topographic influence, that is, below the crests of midocean ridges (Fig. 2). Within this depth range mixing is thought to be associated with tidal forcing over rough bathymetry (Jayne and St. Laurent 2001) and in highly localized flows through passages (Thurnherr et al. 2005) and overflows (Speer and Tziperman 1990; Bryden and Nurser 2003).

Further analysis of the inverse model solutions may help to distinguish mixing sources and characteristics, for instance by the separate consideration of mass, heat, salt, and other tracer fluxes. Freshwater fluxes between low and high latitudes are diagnosed but not interpreted. Some of the model constraints include the effect of eddy transports; however, the role of eddies and their relation to diapycnal fluxes in the closure of the upper cell is not well represented. The global significance of various turbulent transport schemes could be investigated parametrically in the model.

APPENDIX

Initial Reference Level Choices and Constraints for Individual Hydrographic Sections

In this appendix, section-dependent choices of the thermal wind reference level, velocities imposed on the reference level, and constraints on the inverse model solution are presented. Unless explicitly described as a "constraint," the adjustments are applied to the preinverse velocity field and can be freely modified. In many examples, thermal wind with a level of no motion and without additional constraints fails to produce acceptable transports; examples include the Florida Current transport across A5 and the Denmark Strait Overflow in dense layers across Ar18. Additional constraints may be applied locally to groups of station pairs or layers, or to the entire section. An explicit constraint on one section will propagate into adjacent sections, owing to the imposed property conservation in the boxes. The constrained transport in the inverse solution has to have a smaller error range than that on the given constraint itself.

a. Ar18 (Atlantic: Denmark Strait)

Thermal wind was calculated relative to a bottom reference level. The following constraints were imposed to reproduce a more realistic flow structure (LS03): zero net mass exchange between subpolar Atlantic and Nordic seas (0 ± 0.35 Sv across Ar18 + Iceland–Scotland Ridge sections); a Denmark Strait overflow with 2.0 ± 0.2 Sv southward for $\gamma^n > 28.14$, and 0.9 ± 0.1 Sv southward for $28.01 < \gamma^n < 28.14$ (Girton et al. 2001); polar water flow in the East Greenland Current of strength 1.6 ± 0.5 Sv southward in the westernmost 15 station pairs for $\gamma^n < 27.6$ (Malmberg et al. 1972; Mauritzen 1996); and an Irminger Current branch of 0.9 ± 0.4 Sv northward in easternmost five station pairs for $\gamma^n < 27.6$ (Mauritzen 1996).

b. Iceland–Scotland Ridge

A thermal wind reference level $\gamma^n = 27.88$, separating northward-flowing Norwegian Atlantic water from southward-flowing overflow was used. The constraints were a Faroe Bank Channel overflow of 1.4 ± 0.2 Sv southward for $\gamma^n > 28.14$ (Saunders 1990; Mauritzen 1996; Østerhus et al. 1999; Price et al. 2001), an over-

flow across the Iceland–Faroe Rise of 0.85 ± 0.30 Sv southward in the westernmost 14 pairs for $\gamma^n > 27.88$ (Saunders 1990; Mauritzen 1996), a flow of Atlantic water across the Iceland–Faroe Rise of 4.0 ± 0.4 Sv northward in the westernmost 14 pairs for $\gamma^n < 27.88$ (Hansen et al. 1999), and a Norwegian Atlantic Current between the Faroe Islands and Scotland of 3.0 ± 0.4 Sv northward in the easternmost 18 pairs for $\gamma^n < 27.88$ (Gould et al. 1985; Mauritzen 1996; Hansen et al. 1999).

c. Canadian Archipelago

We constructed a simulated hydrographic section from climatology (Gouretski and Jancke 1998). Constraints impose net exchange from the North Pacific to the Atlantic as follows: a Bering Strait throughflow plus net precipitation and river input to the Arctic of 0.9 ± 0.2 Sv net southward (Coachman and Aagaard 1988) and a Bering Strait salt transport of $(26.7 \pm 19) \times 10^6$ kg s^{-1} southward (Wijffels et al. 1992).

d. Ar7 (Atlantic: 56°N)

A thermal wind reference level $\gamma^n = 27.88$ with an East Greenland Current of 15 ± 2 Sv net southward in the westernmost five pairs (Bacon 1997) and 32.2 ± 3.2 Sv net southward in the westernmost seven pairs (Bersch 1995).

e. Ar19 (Atlantic: 48°N)

A thermal wind reference level was set at $\gamma^n = 27.879$. Reference velocities derived from inverted echo sounder measurements (Meinen 2001; Lumpkin et al. 2007) yielded 115 Sv net northward for pairs 4–14 (North Atlantic Current and western half of the Mann eddy). In pairs 15–18 (eastern half Mann eddy) 4.21 cm s^{-1} northward were added to yield 55-Sv net southward transport. Southward flow of 6.59 mm s^{-1} added to all pairs east of pair 18 to yield 2.46 Sv net north from thermal wind, thus balancing the southward Ekman transport. These formed the initial preinversion state—not explicit constraints. No constraints were imposed for this section.

f. Ar16 (Atlantic: Gulf of Cadiz)

A bottom reference level was chosen. Constraints imposed 0 ± 0.25 Sv net exchange between the Atlantic and Mediterranean, a Mediterranean Water Outflow of 2.0 ± 0.5 Sv westward for $27.52 < \gamma^n < 27.88$ (Baringer and Price 1997), and no net flow at densities greater than North Atlantic central water, that is, 0 ± 0.125 Sv net for $\gamma^n > 27.94$ (Baringer and Price 1997).

g. A5 (Atlantic: 24°N)

A bottom reference level for the Florida Straits with uniform reference velocity of 28.5 cm s^{-1} and a 3000-dbar reference level east of the Bahamas (Rintoul and Wunsch 1991). Constraint: Florida Strait transport 31 ± 2 Sv northward (Baringer and Larsen 2001).

h. A8 (Atlantic: 11°S)

Reference levels of 1100 m west of 35.5°W, 3800 m over 17.67°–35.5°W, 2400 m for 10.17°–17.67°W, and 4000 m east of 10.17°W (Speer et al. 1996). Constraints: Antarctic Bottom Water transport is 3.4 ± 1.0 Sv northward for $\gamma^n > 28.12$ (Hall et al. 1997; Mercier and Speer 1998), and there is no net lower deep-water flow east of the Mid-Atlantic Ridge, that is, 0 ± 2 Sv east of 10.5°W for $\gamma^n > 28.1$.

i. A11 (Atlantic: 32°S)

Reference level of $\sigma_3 = 41.58$ (Saunders and King 1995), $\gamma^n = 28.173$–28.178. Constraints: a Malvinas Current of 45 ± 22.5 Sv northward across pairs 1–5 (Saunders and King 1995), an Angola Current of 5 ± 4 Sv southward for pairs 85–89 (Saunders and King 1995); dense flow into the Cape Basin blocked by the Walvis Ridge, or 0 ± 2 Sv across pairs 60–81 for $\gamma^n > 28.175$ (Saunders and King 1995), and an AABW transport into the Argentine Basin of 6 ± 2 Sv northward across pairs 9–45 for $\gamma^n > 28.175$ (Speer and Zenk 1993).

j. Ir6 (Indian: Australia to Indonesia)

A bottom reference level, with the section masked below 100 dbar to prevent spurious net transports in deeper layers. Similar to the Canadian Archipelago section, this section serves to provide the model with reasonable heat and salt transports between ocean basins, with a PIT constrained to be 14 ± 8 Sv westward (Sprintall et al. 2002).

k. I5 (Indian: 32°S)

A bottom reference level in the section interior: 300-m reference level east of 113.5°E (Smith et al. 1991), a 2000-dbar reference level between eastern Natal Valley and 113.5°E (Bryden and Beal 2001), and an LADCP-derived V-shaped reference level west of 113.5°E (Beal and Bryden 1999). "Cul-de-sac" constraints for AABW ($\gamma^n > 28.11$) from Ganachaud (1999) were modified based on L. Beal (2005, personal communication): 0 ± 5-Sv net flow into the Natal Valley (30°–34°W), 0 ± 1 Sv net flow into the Mozambique Basin (35°–46°E), and 0 ± 1 Sv net into the Central

Basin (78°–89°E). Other constraints imposed: a northward deep western boundary current in the Mascarene Basin, fed by flow through the Madagascar–Crozet Basin, 3.15 ± 1.0 Sv northward, 47°–76.5°E, $\gamma^n > 28.13$ (Johnson et al. 1998); a deep northward flow between Broken Plateau and Naturaliste Plateau based on current-meter mooring observations (B. Sloyan 2004, personal communication), 3.7 ± 0.4 Sv northward across 102°–110°E for $\gamma^n > 28.09$; a net Agulhas Current transport of 67 ± 5 Sv southward, west of 31.5°E (Bryden and Beal 2001); and a Leeuwin Current transport of 3.4 ± 1 Sv southward, east of 113.5°E (Feng et al. 2003).

l. Bering Strait

A simulated hydrographic section was constructed from climatology (Gouretski and Jancke 1998). Constraints impose net exchange from the North Pacific to the Arctic: a Bering Strait throughflow 0.8 ± 0.1 Sv net northward (Coachman and Aagaard 1988), and a Bering Strait salt transport of $26.7 \pm 19 \times 10^6$ kg s^{-1} northward (Wijffels et al. 1992).

m. P1 (Pacific: 48°N)

A reference level of $\gamma^n = 28.1$ (Ganachaud 1999).

n. P3 (Pacific: 24°N)

A reference level at 2000 dar (Roemmich and McCallister 1989). Cul-de-sac constraints from Ganachaud (1999): no dense flow into the Okinawa Trough (0 ± 2 Sv for $\gamma^n > 27.52$) at 125°–127°E and no dense flow into the North Philippines Basin (0 ± 2 Sv for $\gamma^n > 28.04$) across 127°–141°E.

o. P6 (Pacific: 32°S)

A reference level at $\gamma^n = 28.125$ (Wijffels et al. 2001). Constraints: no dense flow into the South New Caledonia Trough (0 ± 2 Sv, $\gamma^n > 27.9$) on 162°–168°E (Ganachaud 1999); a deep western boundary current northward against Kermadec Ridge (spanning 169°–179°W), and further constraints of 1 ± 4 Sv for $27.88 < \gamma^n < 28.06$, 8.8 ± 2.0 Sv for $28.06 < \gamma^n < 28.2$, and 6.0 ± 2.0 Sv for $\gamma^n > 28.2$ (Wijffels et al. 2001); a deep ($\gamma^n > 27.9$) flow in the Tasman Sea (Wijffels et al. 2001) along with 0.5 ± 0.5 Sv northward over 150°–160°E, 0 ± 0.5 Sv at 160°–173°E, and 0 ± 0.5 Sv across 173°–180°E; and a deep ($\gamma^n > 28.05$) flow northward in the Eastern Basin (Wijffels et al. 2001) with 0.75 ± 0.75 Sv (northward) across 70°–110°W.

p. S4 (Southern: Circumpolar 62°S)

The S4 circumpolar section was constructed as a composite of WOCE-era sections and casts extracted from the WOCE Southern Ocean Atlas hydrographic dataset (more information is available online at http://woceatlas.tamu.edu/) and tabulated in Table 1. Antarctic surface water and Lower Circumpolar Deep Water ($27.98 < \gamma^n < 28.27$) northward exports, inferred from chlorofluorocarbon observations (Orsi et al. 2002), were applied as constraints. These transports were 3.6 ± 1.8 Sv, Indo–Pacific (30.0°E–70.1°W); 5.9 ± 2.9 Sv, Atlantic (55.2°W–30.0°E). Northward bottomwater ($\gamma^n > 28.27$) transports were also constrained (Orsi et al. 2002): 3.2 ± 1.6 Sv in the Indo–Pacific and 4.9 ± 2.5 Sv in the Atlantic. A deep western boundary current was constrained to be against the Kerguelen Plateau, 38 ± 12 Sv northward (Donohue et al. 1999), $\gamma^n > 28.14$, at 82.8°–106°E.

q. A21 (Southern: Drake Passage)

A bottom reference level with 2 mm s^{-1} uniform eastward reference velocity. A constraint required 130 ± 7-Sv net eastward flow (Whitworth et al. 1982).

r. I6 (Southern: 30°E, Antarctica to South Africa)

A reference level $\gamma^n = 28.292$ (or bottom, if that density not present) with 2.2 mm s^{-1} eastward flow added to yield 140 Sv eastward before inversion.

s. Sr3 (Southern: 143°E, Antarctica to Tasmania)

A reference level $\gamma^n = 28.292$ (or bottom, if that density not present) with 2 mm s^{-1} eastward flow added to yield 155 Sv eastward before inversion.

t. Sr4 (Southern: Weddell Sea)

A reference level at $\gamma^n = 28.292$. Constraints derived from several current-meter arrays (data provided by E. Fahrbach 2003, personal communication): a western boundary current (west of 47.9°W) of 3.26 ± 1.43 Sv northward for $\gamma^n < 28.18$, 11.2 ± 9.2 Sv northward for $28.18 < \gamma^n < 28.27$, and 11.5 ± 8.8 Sv northward for $\gamma^n > 28.27$. Across 41.5°–47.9°W we constrain 2.1 ± 0.1 Sv northward for $\gamma^n < 28.18$ and 5.3 ± 9.5 Sv northward for $\gamma^n > 28.27$. Across 16.8°–41.5°W we constrain 0 ± 0.82 Sv for $\gamma^n < 28.18$, 1.9 ± 1.9 Sv southward for $28.18 < \gamma^n < 28.27$, and 0.9 ± 21.3 Sv northward for $\gamma^n > 28.27$. An eastern boundary current or flow (east of 16.8°W) was constrained to be 11.1 ± 6.0 Sv southward for $\gamma^n < 28.18$, 10.8 ± 7.9 Sv southward for $28.18 < \gamma^n < 28.27$, and 12.9 ± 14.4 Sv southward for $\gamma^n > 28.27$.

REFERENCES

Bacon, S., 1997: Circulation and fluxes in the North Atlantic between Greenland and Ireland. *J. Phys. Oceanogr.,* **27,** 1420–1435.

Baringer, M. O., and J. F. Price, 1997: Mixing and spreading of the Mediterranean outflow. *J. Phys. Oceanogr.,* **27,** 1654–1692.

——, and J. C. Larsen, 2001: Sixteen years of Florida Current transport at 27°N. *Geophys. Res. Lett.,* **28** (16), 3179–3182.

Beal, L., and H. L. Bryden, 1999: The velocity and vorticity structure of the Agulhas Current at 32°S. *J. Geophys. Res.,* **104,** 5151–5176.

Bersch, M., 1995: On the circulation of the northeastern North Atlantic. *Deep-Sea Res.,* **42A,** 1583–1607.

Bryden, H. L., and L. Beal, 2001: Role of the Agulhas Current in Indian Ocean circulation and associated heat and freshwater fluxes. *Deep-Sea Res. I,* **48,** 1821–1845.

——, and A. J. G. Nurser, 2003: Effects of strait mixing on ocean stratification. *J. Phys. Oceanogr.,* **33,** 1870–1872.

Coachman, L., and K. Aagaard, 1988: Transports through Bering Strait: Annual and interannual variability. *J. Geophys. Res.,* **93,** 15 535–15 539.

da Silva, A. M., C. C. Young, and S. Levitus, 1994: *Algorithms and Procedures.* Vol. 1, *Atlas of Surface Marine Data 1994,* NOAA Atlas NESDIS 1, 51 pp.

Donohue, K. A., G. E. Hufford, and M. S. McCartney, 1999: Sources and transport of the deep western boundary current east of the Kerguelen Plateau. *Geophys. Res. Lett.,* **26** (7), 851–854.

Farbach, E., G. Rohardt, M. Shröder, and V. Strass, 1995: The Weddell Gyre Study 1989–1993. *International WOCE Newsletter,* No. 18, WOCE International Project Office, Southampton, United Kingdom, 6–9.

Feng, M., G. Meyers, A. Pearce, and S. Wijffels, 2003: Annual and interannual variations of the Leeuwin Current at 32°S. *J. Geophys. Res.,* **108,** 3355, doi:10.1029/2002JC001763.

Ganachaud, A., 1999: Large-scale oceanic circulation and fluxes of freshwater, heat, nutrients and oxygen. Ph.D. thesis, Massachusetts Institute of Technology–Woods Hole Oceanographic Institute Joint Program, 249 pp.

——, 2003a: Error budget of inverse box models: The North Atlantic. *J. Atmos. Oceanic Technol.,* **20,** 1641–1655.

——, 2003b: Large-scale mass transports, water mass formation, and diffusivities estimated from World Ocean Circulation Experiment (WOCE) hydrographic data. *J. Geophys. Res.,* **108,** 3213, doi:10.1029/2002JC001565.

——, and C. Wunsch, 2000: Improved estimates of global ocean circulation, heat transport and mixing from hydrographic data. *Nature,* **408,** 453–457.

Garabato, A. C. N., D. P. Stevens, and K. J. Heywood, 2003: Water mass conversion, fluxes, and mixing in the Scotia Sea diagnosed by an inverse model. *J. Phys. Oceanogr.,* **33,** 2565–2587.

Garnier, E., B. Barnier, L. Siefridt, and K. Beranger, 2000: Investigating the 15 years air–sea flux climatology from the ECMWF re-analysis project as a surface boundary condition for ocean models. *Int. J. Climatol.,* **20,** 1653–1673.

Girton, J. B., T. B. Sanford, and R. H. Käse, 2001: Synoptic sections of the Denmark Strait overflow. *Geophys. Res. Lett.,* **28,** 1619–1622.

Gnanadesikan, A., 1999: A simple predictive model for the structure of the oceanic pycnocline. *Science,* **283,** 2077–2079.

Gould, W. J., L. Loynes, and J. Backhaus, 1985: Seasonality in slope current transports N.W. of Shetland. ICES Hydrography Committee C.M. 1985/C:7, 13 pp.

Gouretski, V., and K. Jancke, 1998: A new climatology for the World Ocean. WOCE Hydrographic Program Special Analysis Centre Tech. Rep. 3, WOCE Rep. 162/98, Hamburg, Germany, 40 pp.

Grist, J. P., and S. A. Josey, 2003: Inverse analysis adjustment of the SOC air–sea flux climatology using ocean heat transport constraints. *J. Climate,* **16,** 3274–3295.

Hall, M. M., M. McCartney, and J. A. Whitehead, 1997: Antarctic bottom water flux in the equatorial western Atlantic. *J. Phys. Oceanogr.,* **27,** 1903–1926.

Hansen, B., K. M. H. Larsen, S. Østerhus, B. Turrell, and S. Jónsson, 1999: The Atlantic water inflow to the Nordic Seas. *International WOCE Newsletter,* No. 35, WOCE International Project Office, Southampton, United Kingdom, 33–35.

Jackett, D. R., and T. J. McDougall, 1997: A neutral density variable for the world's oceans. *J. Phys. Oceanogr.,* **27,** 237–263.

Jayne, S. R., and L. St. Laurent, 2001: Parameterizing tidal dissipation over rough topography. *Geophys. Res. Lett.,* **28,** 811–814.

Johnson, G. C., D. L. Musgrave, B. A. Warren, A. Ffield, and D. B. Olson, 1998: Flow of bottom and deep water in the Amirante Passage and Mascarene Basin. *J. Geophys. Res.,* **103,** 30 973–30 984.

Josey, S. A., 2001: A comparison of ECMWF, NCEP–NCAR, and SOC surface heat fluxes with moored buoy measurements in the subduction region of the Northeast Atlantic. *J. Climate,* **14,** 1780–1789.

——, E. C. Kent, and P. K. Taylor, 1998: The Southampton Oceanography Centre (SOC) ocean–atmosphere heat, momentum and freshwater flux atlas. Southampton Oceanography Centre Rep. 6, 30 pp.

——, ——, and ——, 1999: New insights into the ocean heat budget closure problem from analysis of the SOC air–sea flux climatology. *J. Climate,* **12,** 2856–2880.

Khatiwala, S., P. Schosser, and M. Visbeck, 2002: Rates and mechanisms of water mass transformation in the Labrador Sea as inferred from tracer observations. *J. Phys. Oceanogr.,* **32,** 666–686.

Kunze, E., E. Firing, J. M. Hummon, T. K. Chereskin, and A. M. Thurnherr, 2006: Global abyssal mixing inferred from lowered ADCP shear and CTD strain profiles. *J. Phys. Oceanogr.,* **36,** 1553–1576.

Levitus, S., and T. P. Boyer, 1994: *Temperature.* Vol. 4, *World Ocean Atlas 1994,* NOAA Atlas NESDIS 4, 117 pp.

Lumpkin, R., and K. Speer, 2003: Large-scale vertical and horizontal circulation in the North Atlantic Ocean. *J. Phys. Oceanogr.,* **33,** 1902–1920.

——, ——, and K. P. Koltermann, 2007: Transport across 48°N in the Atlantic Ocean. *J. Phys. Oceanogr.,* in press.

Malmberg, S. A., H. G. Gade, and H. E. Sweers, 1972: Current velocities and volume transports in the East Greenland Current off Cape Nordenskjold in August–September 1965. *Proc. Int. Sea Ice Conf.,* Reykjavík, Iceland, National Research Council of Iceland, 130–139.

Mauritzen, C., 1996: Production of dense overflow waters feeding the North Atlantic across the Greenland–Scotland Ridge. *Deep-Sea Res.,* **43A,** 769–835.

Meinen, C. S., 2001: Structure of the North Atlantic Current in stream-coordinates and the circulation in the Newfoundland Basin. *Deep-Sea Res.,* **48,** 1553–1580.

Mercier, H., and K. G. Speer, 1998: Transport of bottom water in the Romanche Fracture Zone and the Chain Fracture Zone. *J. Phys. Oceanogr.,* **28,** 779–790.

Munk, W., and C. Wunsch, 1998: Abyssal recipes II: Energetics of tidal and wind mixing. *Deep-Sea Res.* **45,** 1976–2000.

Orsi, A. H., W. M. Smethie Jr., and J. L. Bullister, 2002: On the total input of Antarctic waters to the deep ocean: A preliminary estimate from chlorofluorocarbon measurements. *J. Geophys. Res.,* **107,** 3122, doi:10.1029/2001JC000976.

Østerhus, S., B. Hansen, R. Kristiansen, and P. Lundberg, 1999: The overflow through the Faroe Bank Channel. *International WOCE Newsletter,* No. 35, WOCE International Project Office, Southampton, United Kingdom, 35–37.

Price, J. F., and M. Baringer, 1994: Outflows and deep-water production by marginal seas. *Prog. Oceanogr.,* **33,** 161–200.

——, T. Sanford, C. Mauritzen, and M. Prater, cited 2001: A report of XCP and CTD data taken during June 2001, RRS Discovery cruise 247B: A process study of the Faroe Bank Channel overflow. [Available online at http://www.whoi.edu/science/PO/people/jprice/oflow/FBC.pdf.]

Rintoul, S. R., and C. Wunsch, 1991: Mass, heat, oxygen and nutrient fluxes and budgets in the North Atlantic Ocean. *Deep-Sea Res.,* **38** (suppl.), S355–S377.

Robbins, P. E., and J. M. Toole, 1997: The dissolved silica budget as a constraint on the meridional overturning circulation in the Indian Ocean. *Deep-Sea Res.,* **41,** 143–168.

Roemmich, D. L., and T. McCallister, 1989: Large scale circulation of the North Pacific Ocean. *Prog. Oceanogr.,* **22,** 171–204.

Saunders, P. M., 1990: Cold outflow from the Faroe Bank Channel. *J. Phys. Oceanogr.,* **20,** 29–43.

——, and B. A. King, 1995: Bottom currents derived from a shipborne ADCP on WOCE cruise A11 in the South Atlantic. *J. Phys. Oceanogr.,* **25,** 329–347.

Schmitz, W. J., Jr., 1996: On the World Ocean circulation. Vol. II: The Pacific and Indian Oceans/A global update. Tech. Rep. WHOI-96-O8, Woods Hole Oceanographic Institute, 237 pp.

Sloyan, B. M., and S. R. Rintoul, 2001: The Southern Ocean limb of the global deep overturning circulation. *J. Phys. Oceanogr.,* **31,** 143–173.

Smith, R. L., A. Huyer, J. S. Godfrey, and J. A. Church, 1991: The Leeuwin Current off Western Australia, 1986–1987. *J. Phys. Oceanogr.,* **21,** 323–345.

Speer, K., 1997: A note on average cross-isopycnal mixing in the North Atlantic Ocean. *Deep-Sea Res.,* **44,** 1981–1990.

——, and E. Tziperman, 1990: Convection from a source in an ocean basin. *Deep-Sea Res.,* **37,** 431–446.

——, and W. Zenk, 1993: The flow of Antarctic Bottom Water into the Brazil Basin. *J. Phys. Oceanogr.,* **23,** 2667–2682.

——, J. Holfort, T. Reynaud, and G. Siedler, 1996: South Atlantic heat transport at 11°S. *The South Atlantic: Present and Past Circulation,* G. Wefer et al., Eds., Springer-Verlag, 105–120.

——, S. R. Rintoul, and B. Sloyan, 2000: The diabatic Deacon cell. *J. Phys. Oceanogr.,* **30,** 3212–3222.

Speich, S., B. Blanke, P. de Vries, S. Drijfhouté, K. Döös, A. Ganachaud, and R. Marsh, 2002: Tasman leakage: A new route in the global ocean conveyor belt. *Geophys. Res. Lett.,* **29,** 1416, doi:10.1029/2001GL014586.

Sprintall, J., S. Wijffels, T. Chareskin, and N. Bray, 2002: The JADE and WOCE I10/IR6 throughflow sections in the southeast Indian Ocean. Part 2: Velocity and transports. *Deep-Sea Res.,* **49,** 1363–1389.

Talley, L. D., J. L. Reid, and P. E. Robbins, 2003: Data-based meridional overturning streamfunctions for the global ocean. *J. Climate,* **16,** 3213–3226.

Thurnherr, A. M., L. C. St. Laurent, K. G. Speer, J. M. Toole, and J. R. Ledwell, 2005: Mixing associated with sills in a canyon on the midocean ridge flank. *J. Phys. Oceanogr.,* **35,** 1370–1381.

Toole, J. M., K. L. Polzin, and R. W. Schmitt, 1994: Estimates of diapycnal mixing in the abyssal ocean. *Science,* **264,** 1120–1123.

Wacongne, S., K. Speer, R. Lumpkin, and V. Sadoulet, 2003: Warm water formation in the midst of the Southern Ocean. Preprints, *Seventh Conf. on Polar Meteorology and Oceanography and Joint Symp. on High-Latitude Climate Variations,* Hyannis, MA, Amer. Meteor. Soc., CD-ROM, 5.19.

Warren, B. A., J. H. LaCasce, and P. E. Robbins, 1996: On the obscurantist physics of "form drag" in theorizing about the Circumpolar Current. *J. Phys. Oceanogr.,* **26,** 2297–2301.

WGASF, 2001: Intercomparison and validation of ocean–atmosphere energy flux fields. Final Rep. of the Joint WCRP/SCOR Working Group on Air–Sea Fluxes, WCRP Series Rep. 112, 296 pp.

Whitworth, T., III, W. D. Nowlin Jr., and S. J. Worley, 1982: The net transport of the Antarctic Circumpolar Current through Drake Passage. *J. Phys. Oceanogr.,* **12,** 960–971.

Wijffels, S. E., R. W. Schmitt, H. L. Bryden, and A. Stigebrandt, 1992: Transports of freshwater by the oceans. *J. Phys. Oceanogr.,* **22,** 155–162.

——, J. M. Toole, and R. Davis, 2001: Revisiting the South Pacific subtropical circulation: A synthesis of World Ocean Circulation Experiment observations along 32°S. *J. Geophys. Res.,* **106** (C9), 19 481–19 514.

Wunsch, C., 1996: *The Ocean Circulation Inverse Problem.* Cambridge University Press, 442 pp.

Yaremchuk, M., D. Nechaev, J. Schroter, and E. Fahrbach, 1998: A dynamically consistent analysis of circulation and transports in the southwestern Weddell Sea. *Ann. Geophys.,* **16,** 1024–1038.

Zhang, H.-M., and L. Talley, 1998: Heat and buoyancy budgets and mixing rates in the upper thermocline of the Indian and Global Oceans. *J. Phys. Oceanogr.,* **28,** 1961–1978.